



B-Mode Photoacoustic Imaging Using Linear Array: Numerical Study for Forward-Backward Minimum Variance Beamformer Combined with Delay-Multiply-and-Sum

M. Mozaffarzadeh¹, S. A. O. Izadi Avanj^{2*}, H. R. Jashnani³

¹ Biomedical Engineering, Tarbiat Modares University, Tehran, Iran

² Department of Electrical Engineering, Shahid Sattari Aeronautical University of Science and Technology, Tehran, Iran

³ Department of Air traffic Engineering, Shahid Sattari Aeronautical University of Science and Technology, Tehran, Iran

ABSTRACT: Photoacoustic imaging (PAI) is a promising medical imaging modality which provides the resolution of Ultrasound (US) and the contrast of optical imaging modalities. One of the most important challenges in PAI is image formation, especially in the case that a linear-array US transducer is used for data acquisition. This is due to the fact that in the linear-array scenario, there is only 60 degrees view-angle available to detect the photoacoustic waves. Because of the nature of photoacoustic waves, the image formation procedure is inherently a limited angle-view problem. Delay-and-Sum (DAS) is the most prevalent beamforming algorithm in PAI due to its simple implementation, but it provides low-quality images. One of the alternatives is Minimum Variance (MV) and its derivatives. In this paper, we introduce a novel beamforming algorithm based on the combination of Forward-Backward MV (FBMV) and Delay-Multiply-and-Sum (DMAS) beamforming algorithms, called DMAS_FBMV. It is shown that the FBMV can be integrated into the expansion of the DMAS algorithm. The proposed method is evaluated numerically. The results demonstrate that the DMAS_FBMV significantly outperforms the FBMV in terms of sidelobes (12 dB improvement at 45 mm). Quantitative metrics such as Signal-to-Noise and Full-Width-Half-Maximum are calculated for a better evaluation.

Review History:

Received: 29 January 2018

Revised: 17 February 2019

Accepted: 4 March 2019

Available Online: 4 March 2019

Keywords:

Photoacoustic imaging

image formation

beamforming

linear-array imaging

contrast improvement

1- Introduction

Photoacoustic imaging (PAI) is a novel medical imaging modality which combines the contrast of optical and the resolution of Ultrasound (US) imaging [1]. In PAI, the target is illuminated with a short electromagnetic pulse (laser, infrared light, radio wave or Microwave). Then, based on the thermoelastic effects, the transient Photoacoustic (PA) waves are generated [2].

Over the past few years, PAI has been extensively investigated in different studies, such as monitoring oxygenation in blood vessels [3], breast tumor detection [4], cancer staging [1] and ocular imaging [5]. When the PA signals are recorded by US transducers, mathematics can be used to form an image. The PA images illustrate the optical absorption distribution map of the tissue. There are a large number of publications focused on this field of study [6-9]. In [10], a time-domain quantitative photoacoustic image reconstruction algorithm has been used to form PA images. An automatic sound selection based on the maximization of the sharpness of the reconstructed image has been proposed in [11]. Acoustic heterogeneity has been a matter of study in multiple studies, as well [12-15].

PAI is a multiscale imaging modality, and different configurations can be achieved [16]. For data detection, linear, arc, and circular transducer arrays can be used [17]. The focus of this paper is on the linear-array scenario [18-22].

In linear-array PAI, beamforming algorithms can be used for image reconstruction. Beamformers investigated in US imaging can also be used in PAI, with some modifications [23-25]. In PAI, the transmission part is concerned with the laser illumination, but in US imaging, the transmission is

done through a US waveform. Delay-and-Sum (DAS) is the most commonly used beamforming algorithm in US and PAI. However, it leads to low-quality images due to its blindness [23-25]. Delay-Multiply-and-Sum (DMAS), which uses a correlation process to reconstruct images, was introduced for linear-array US imaging [26]. In [23-25], it was shown that the contrast achieved by the DMAS is not good enough for PAI, especially in the presence of a high level of noise. To address this problem, Double-Stage DMAS (DS-DMAS) was proposed [23-25]. This beamformer was also utilized for US imaging [24], and LED-based PAI systems [25].

While DMAS provides a better contrast compared to DAS, it does not improve the resolution. On the other hand, when it comes to resolution, the Minimum Variance (MV) algorithms are great options. However, MV results in high sidelobes [27, 28]. To address the incapacities in both the MV and DMAS, these beamformers were combined [19, 29]. This beamformer was called MV-Based DMAS (MVB-DMAS) and the superiority of this method was proved in previous publications [29]. In addition, the eigenspace version of the MVB-DMAS was introduced, and the results showed the superiority of this beamformer compared to DMAS and eigenspace MV (EIBMV) [19].

In this paper, we investigate the performance of the combination of the Forward-Backward MV (FBMV) beamforming algorithm and DMAS. The proposed algorithm is the so-called DMAS_FBMV [30]. It is shown that inside the expansion of the DMAS algebra, there are terms which can be interpreted as DAS. To improve the image quality, it is proposed to implement FBMV instead of the DAS terms. Results are promising, and the superiority of the proposed method is proved.

Corresponding author, E-mail:

The rest of the paper is as follows. In section 2, the background of PAI and the methods used are illustrated. The results are presented in section 3. Section 4 contains the discussion. Finally, the conclusion is presented in section 5.

2- Theoretical or experimental modeling

In this section, the basic concept of PAI, beamformers, and the proposed method are presented.

2- 1- Photoacoustic

In typical PAI, waves are propagated based on the thermoelastic expansion, and US transducers are utilized to record the generated signals. Under the thermal confinement, inhomogeneous optical absorption medium, and acoustic homogeneity, the pressure $P(r, t)$, at the time t and the position r , resulted from heat sources $H(r, t)$, obeys Eq. (1):

$$c^2 \nabla^2 p(r, t) - \frac{\partial^2}{\partial t^2} p(r, t) = -\Gamma(r) \frac{H(r, t)}{t}, \quad (1)$$

where β is the isobaric volume expansion, $\Gamma(r) = \beta c^2 / C_p$ is the Gruneisen parameter, C_p is the heat capacity, and c is the speed of sound [7]. The heat function can be written as follows:

$$H(r, t) = A(r)I(t), \quad (2)$$

where $A(r)$ and $I(t)$ are the spatial absorption and the temporal illumination functions, respectively [9]. Given $I(t) = \delta(t)$, $P(r_0, t)$, which is the obtained pressure at the time t and the detector position r_0 , can be written as follows:

$$p(r_0, t) = \frac{1}{c} \frac{\partial}{\partial t} \iiint d^3r D(r) \frac{\delta(ct - |r_0 - r|)}{4\pi |r_0 - r|}, \quad (3)$$

where $D(r) = \Gamma(r)A(r)$. Eq. (3) is known as the forward problem in PAI. The backward problem is related to the reconstruction of $A(r)$ using recorded PA waves. Based on the assumptions and simplifications explained in [6], the PA image is obtained by Eq. (4):

$$D(\rho, \phi, z) = -\frac{1}{2\pi c^2} \iint ds_0 [n \cdot n_0] \frac{1}{t} \frac{\partial p(r_0, t)}{\partial t} \Big|_{t=|r-r_0|/c}, \quad (4)$$

where

$$n \cdot n_0 = \frac{(\rho - \rho_0)}{(r - r_0)} = \sqrt{\frac{\rho^2 + \rho_0^2 + 2\rho\rho_0 \cos(\phi - \phi_0)}{(r - r_0)^2}} = \sqrt{1 - \frac{(z_0 - z)^2}{(r - r_0)^2}}, \quad (5)$$

$ds_0 = \rho_0 d\phi_0 dz_0$ and ρ_0 are the projection of r and r_0 on the z plane, respectively [26].

2- 2- beamforming algorithms

The most basic beamformer for linear-array PA/US imaging is DAS. The formula of DAS is as follows:

$$y_{DAS}(k) = \sum_{i=1}^M x_i(k - \Delta_i), \quad (6)$$

where M is the number of array elements, y_{DAS} is the output of the beamformer, and $x_i(k)$ and Δ_i are the recorded signals and the corresponding time delay for element i , respectively.

Eq. (6) results in low-quality images. DMAS (introduced by Matrone *et al.* [26]) shows that a correlation process can be used to improve the quality of the formed images, compared to DAS. DMAS formula is as follows:

$$y_{DMAS}(k) = \sum_{i=1}^{M-1} \sum_{j=i+1}^M x_i(k - \Delta_i) x_j(k - \Delta_j). \quad (7)$$

To solve the dimensionally squared problem of (7), the following formulas are introduced in [26].

$$\hat{x}_{ij}(k) = \text{sign}[x_i(k - \Delta_i) x_j(k - \Delta_j)] \sqrt{|x_i(k - \Delta_i) x_j(k - \Delta_j)|}, \quad (8)$$

for $i \leq j \leq M$

$$y_{DMAS}(k) = \sum_{i=1}^{M-1} \sum_{j=i+1}^M \hat{x}_{ij}(k). \quad (9)$$

More information and explanations about the DMAS algorithm can be found in [26]. Although it is proved that DMAS outperforms DAS in terms of resolution and level of sidelobes, its resolution is not satisfying in comparison with Minimum Variance-Based algorithms [19, 29]. In the following, it is shown that we can integrate the FBMV adaptive beamformer into the DMAS formula expansion.

2- 3- Proposed method

In this paper, it is proposed to use the FBMV adaptive beamformer instead of the existing DAS algebra inside the DMAS mathematical expansion. To illustrate this, consider the expansion of the DMAS algorithm which can be written as follows:

$$y_{DMAS}(k) = \sum_{i=1}^{M-1} \sum_{j=i+1}^M x_{id}(k) x_{jd}(k) = [x_{1d}(k) x_{2d}(k) + x_{1d}(k) x_{3d}(k) + \dots + x_{1d}(k) x_{Md}(k)] + [x_{2d}(k) x_{3d}(k) + x_{2d}(k) x_{4d}(k) + \dots + x_{2d}(k) x_{Md}(k)] + \dots + [x_{(M-2)d}(k) x_{(M-1)d}(k) + x_{(M-2)d}(k) x_{Md}(k)] + [x_{(M-1)d}(k) x_{Md}(k)] \quad (10)$$

where $x_{id}(k)$ and $x_{jd}(k)$ are delayed detected signals for element i and j , respectively. As can be seen, there is a DAS in every term of the expansion, and it can be used to modify the DMAS beamformer. To illustrate this, consider the following equation:

$$y_{DMAS}(k) = \sum_{i=1}^{M-1} \sum_{j=i+1}^M x_{id}(k) x_{jd}(k) = x_{1d}(k) \underbrace{[x_{2d}(k) + x_{3d}(k) + x_{4d}(k) + \dots + x_{Md}(k)]}_{\text{first term}} + x_{2d}(k) \underbrace{[x_{3d}(k) + x_{4d}(k) + \dots + x_{Md}(k)]}_{\text{second term}} + \dots + x_{(M-2)d}(k) \underbrace{[x_{(M-1)d}(k) + x_{Md}(k)]}_{\text{(M-2)th term}} + \underbrace{[x_{(M-1)d}(k) x_{Md}(k)]}_{\text{(M-1)th term}} \quad (11)$$

In Eq. (11), in every term, there exists a summation procedure which is a type of DAS algorithm. It is proposed to use FBMV adaptive beamformer for each term instead of the DAS. In other words, since DAS is a non-adaptive beamformer and

considers all calculated samples for each element of the array the same as each other, the acquired image by each term is a low-quality image with a high level of sidelobes and broad main lobe. In order to use FBMV instead of every DAS in the expansion, Eq. (11), we need to carry out some modifications and prepare the expansion in Eq. (11). It should be noticed that the quality of covariance matrix estimation in FBMV highly depends on the selected length of subarray. The upper boundary is limited to $M/2$ and the lower boundary to 1. Choosing $L=M/2$ leads to resolution enhancement at the cost of robustness, and $L=1$ leads to resolution reduction and robustness increment. In Eq. (11), each term can be considered as a DAS algorithm with different numbers of elements of the array. In other words, the number of samples of elements contributing to the existing DAS is different in each term, which results from the nature of DMAS algorithm. The limited number of entries in each term causes a problem for FBMV algorithm due to the limited length of the subarray. This problem can be addressed by adding the unavailable elements in each term in order to acquire large enough number of elements so that a high-quality covariance matrix estimation can be obtained. The extra terms, needed to address the problems, are given by:

$$y_{extra}(k) = \sum_{i=M-2}^2 \sum_{j=i-1}^1 x_{id}(k)x_{jd}(k) + y_{extra}^* =$$

$$x_{(M-2)d}(k)[x_{(M-3)d}(k) + x_{(M-4)d}(k) + \dots + x_{2d}(k) + x_{1d}(k)] + \quad (12)$$

$$x_{(M-3)d}(k)[x_{(M-4)d}(k) + x_{(M-5)d}(k) + \dots + x_{2d}(k) + x_{1d}(k)] + \dots +$$

$$x_{3d}(k)[x_{2d}(k) + x_{1d}(k)] + x_{2d}(k)x_{1d}(k) + y_{extra}^*(k),$$

where

$$y_{extra}^*(k) =$$

$$x_{Md}(k)[x_{(M-1)d}(k) + x_{(M-2)d}(k) + \dots + x_{3d}(k) + x_{2d}(k) + x_{1d}(k)] \quad (13)$$

Eq. (12) is used to make the terms in Eq. (11) ready to adopt an FBMV algorithm. Finally, by summing Eq. (12) and Eq. (10), a modified version of DMAS algorithm, namely modified DMAS (MDMAS) is obtained:

$$y_{MDMAS}(k) = y_{DMAS}(k) + y_{extra}(k) = \sum_{i=1}^M \sum_{j=1, j \neq i}^M x_{id}(k)x_{jd}(k) =$$

$$x_{1d}(k) \underbrace{[x_{2d}(k) + x_{3d}(k) + \dots + x_{(M-1)d}(k) + x_{Md}(k)]}_{\text{first term}} +$$

$$x_{2d}(k) \underbrace{[x_{1d}(k) + x_{3d}(k) + \dots + x_{(M-1)d}(k) + x_{Md}(k)]}_{\text{second term}} + \quad (14)$$

$$x_{3d}(k) \underbrace{[x_{1d}(k) + x_{2d}(k) + x_{4d}(k) + \dots + x_{Md}(k)]}_{\text{first term}} + \dots +$$

$$x_{(M-1)d}(k) \underbrace{[x_{1d}(k) + x_{2d}(k) + \dots + x_{(M-2)d}(k) + x_{Md}(k)]}_{\text{first term}} +$$

$$x_{Md}(k) \underbrace{[x_{1d}(k) + x_{2d}(k) + \dots + x_{(M-2)d}(k) + x_{(M-1)d}(k)]}_{\text{Mth term}}.$$

Now, the combination of MDMAS algorithm and FBMV beamformer is mathematically satisfying and instead of every term in Eq. (14), FBMV can be implemented using all entities in each term.

3- Results

3- 1- Point targets

The K-wave Matlab toolbox is used to conduct the numerical study. Eleven 0.1 mm radius spherical absorbers as initial pressure are positioned along the vertical axis every 5 mm beginning 25 mm from the transducer surface. The imaging region is 20 mm in the lateral axis and 80 mm in the vertical axis. A linear-array having $M=128$ elements operating at 5 MHz central frequency and 77% fractional bandwidth detects the PA signals generated from the defined initial pressures. The speed of sound is assumed to be 1540 m/s during the simulations. The sampling frequency is 50 MHz, subarray length $L=M/2$, $K=2$ and $\Delta=1/100L$ for all the simulations. Also, a band-pass filter is applied by a Tukey window ($\alpha=0.5$) to the beamformed signal spectra, covering 6-16 MHz, to pass the necessary information.

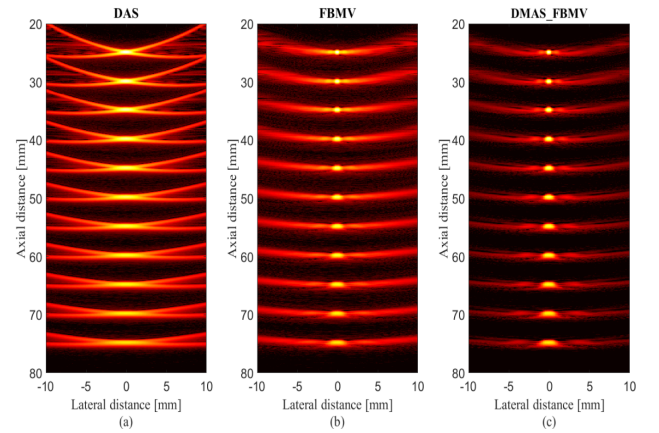


Fig. 1. Images of the simulated point targets phantom using the linear-array transducer. (a) DAS, (b) FBMV, and (c) DMAS_FBMV. All images are shown with a dynamic range of 60 dB. Noise was added to the detected signals considering an SNR of 50 dB.

The reconstructed images using the concerned beamformers are shown in Fig. 1. As can be seen, the formed image using DAS has a low quality, and the point targets are not well-detectable. FBMV improves the image quality by providing a higher resolution, but the levels of sidelobe are still degrading the image quality. As demonstrated in Fig. 1(c), the proposed method reduces the sidelobes compared to the FBMV while the resolution is retained. To have a better evaluation, the lateral variations of the images shown in Fig. 1 are presented in Fig. 2. As demonstrated, the MV-based algorithms provide a higher resolution (narrower width of main lobe) compared to DAS. It should be noted that the sidelobes of FBMV are not satisfying. The proposed method reduces the sidelobes of FBMV which results in a higher contrast. For instance, considering the depth of 45 mm, it can be seen that FBMV and DMAS_FBMV results in about -24 dB and -36 dB sidelobes, respectively. In other words, DMAS_FBMV degrades the sidelobes about -12 dB in comparison with FBMV. To compare the performance of the beamformers quantitatively, the full-width-half-maximum (FWHM) in -6 dB and signal-to-noise ratio (SNR) are calculated using the point targets in the reconstructed images. The SNR formula is presented in references [23, 24]. SNRs and FWHMs are shown in Table 1 and Table 2, respectively. As can be seen, in all the depths, the proposed method outperforms the FBMV and DAS. Considering

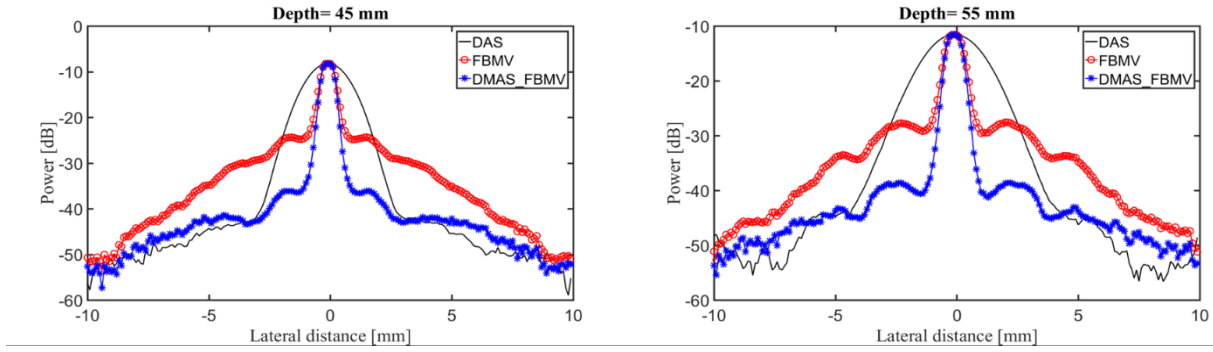


Fig. 2. Lateral variations of DAS, FBMV, and DMAS_FBMV at the depths of (a) 40 mm and (b) 55 mm.

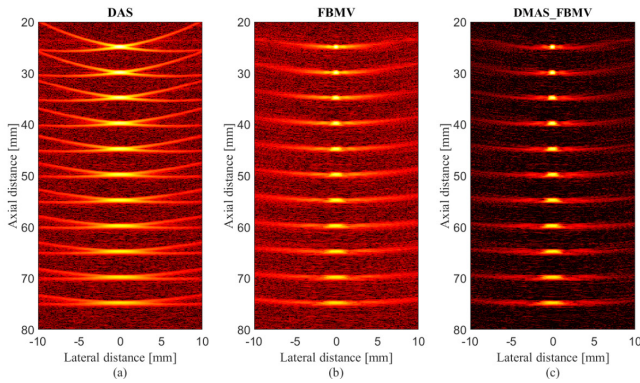


Fig. 3. Images of the simulated point targets phantom using the linear-array transducer. (a) DAS, (b) FBMV, and (c) DMAS_FBMV. All images are shown with a dynamic range of 60 dB. Noise was added to the detected signals considering an SNR of 20 dB.

Table 1, at the depth of 25 mm, it can be seen that DMAS_FBMV results in 26.98 dB and 5.44 dB improvement, respectively in the term of SNR, compared to DAS and FBMV. Considering Table 2, it is demonstrated that DMAS_FBMV leads to a narrower width of main lobe (in -6 dB), in comparison with other methods. To evaluate the performance of the proposed method in the term of noise suppression, noise was added to the detected PA signals considering an SNR of 20 dB. The reconstructed images are shown in Fig. 3. The proposed method leads to a higher noise suppression compared to other methods since the background of the image shown in Fig. 3(c) is darker. Thus, a higher SNR and noise suppression are achieved using the proposed method by comparing the results in Table 1, Fig. 1 and Fig. 3.

3- 2- Cyst Targets

To evaluate the beamformers under the cyst targets, a cyst is positioned at the depth of 15 mm. The PA signals are recorded using the same linear-array used for the point target simulation.

Table 1. SNR (dB) values at different depths.

Beamformer	DAS	FBMV	DMAS_FBMV
Depth (mm)			
25	34.71	56.25	61.69
35	34.11	51.74	54.29
45	32.71	43.90	44.81
55	29.90	40.63	42.56
65	26.22	33.09	33.95
75	22.93	27.88	28.25

Table 2. FWHM (mm) values (in -6 dB) at the different depths.

Beamformer	DAS	FBMV	DMAS_FBMV
Depth (mm)			
25	1.10	0.33	0.30
35	1.63	0.60	0.53
45	2.28	0.79	0.71
55	3.06	1.00	0.88
65	3.70	1.31	1.19
75	4.87	1.54	1.42

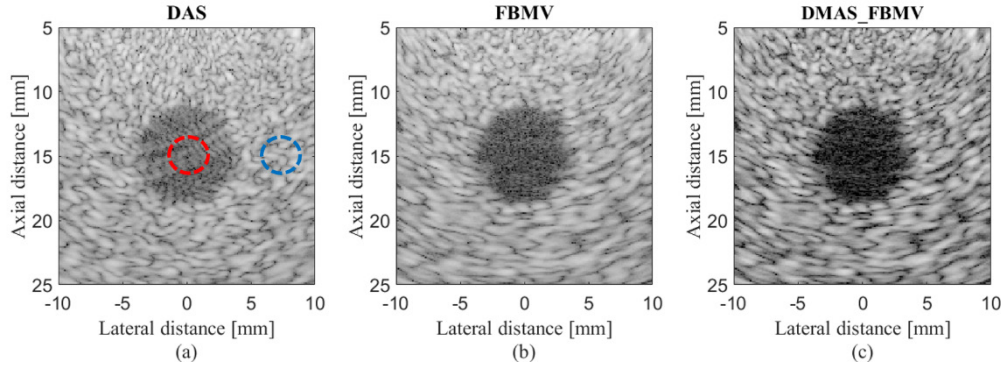


Fig. 4. Images of the simulated cyst targets phantom using the linear-array transducer. (a) DAS, (b) FBMV, and (c) DMAS_FBMV. All images are shown with a dynamic range of 60 dB. Noise was added to the detected signals considering an SNR of 50 dB.

All the parameters are the same as what is mentioned in section 3.1. The reconstructed PA images are shown in Fig. 4. As can be observed, sidelobes and artifacts highly affect the area inside the cyst. To put it more simply, DAS results in a low contrast image. FBMV degrades the sidelobes further and leads to a higher contrast compared to DAS. In addition, the higher resolution of FBMV is clear considering the edges of the cyst in the images (Fig. 4). For further evaluation, the Contrast Ratio (CR) metric was calculated. The formula of CR is as follows:

$$CR = 20 \log_{10} \left(\frac{\mu_{cyst}}{\mu_{bck}} \right), \quad (15)$$

where μ_{cyst} and μ_{bck} are the mean of image intensity before log compression inside the red and blue dotted circle in Fig. 4(a), respectively. The CR for DAS, FBMV and DMAS_FBMV is about -12.85 dB, -19.31 dB and -26.59 dB, respectively. In other words, the proposed method improves the CR for about 13.74 dB and 7.28 dB, respectively compared to DAS and FBMV.

4- Discussion

The proposed algorithm in this paper is the combination of two beamformer. In [29], the combination of MV and DMAS is proposed (so-called MVB-DMAS). In terms of contrast, DMAS_FBMV outperforms MVB-DMAS since FBMV outperforms MV, as concluded in [30]. However, both of these algorithms are sensitive to imaging noise and may fail in the presence of high levels of noise. Compared to the DS-DMAS [23-25], the DMAS_FBMV provides a better resolution (narrower width of main lobe).

As was demonstrated by the qualitative and quantitative results, the proposed method (DMAS_FBMV) outperforms DAS and FBMV in all the terms. However, it should be noticed that the superior performance of the proposed method is achieved at the expense of a higher computational burden due to the combination of DMAS and FBMV. Worthy of note, it will still be in the same order of FBMV. As can be seen in the previous section, we have compared the proposed method with the method it has been derived from; FBMV. Under any condition, if the performance of the FBMV is increased, the performance of the proposed method will be increased, as well. The combinational method proposed in this paper was also used for MV and EIBMV beamforming methods (please refer to references [19, 29]), and a higher performance of this concept was also proved using numerical and experimental

studies in the relevant papers.

It should be noticed that the proposed method is composed of two other beamformers. In other words, it is a combination of FBMV and DMAS. Since it uses the procedure of the FBMV, in the case that we are facing a high level of noise, the performance of the proposed method would be decreased. In fact, the presence of noise highly affects the quality of the estimated covariance matrix which finally, affects the image quality.

The computational complexity of DAS, DMAS, and EIBMV is in the order of M , M^2 and M^3 , respectively. To have the proposed method implemented, we need to implement DMAS and FBMV. The computational complexity of the proposed method is in the order of $O(M^3)$, which results from the computational complexity of FBMV. Since we also have a DMAS in the proposed method, the overall computational complexity of FBMV is higher than DMAS and FBMV. The images which are shown in Fig. 3 have 800×200 pixels density. To generate these images using DAS, FBMV, and DMAS_FBMV, it takes 1.2 s, 197.1 s and 210 s, respectively. As a result, FBMV_DMAS is not a proper option for real-time imaging.

5- Conclusion

PAI provides anatomical, structural, and molecular information making it one of the most important imaging modalities, especially linear-array PAI. The most challenging problem in linear-array PAI is image formation due to the fact that a limited number of angles (sensors covering the target of imaging) are available. In this paper, a novel image reconstruction algorithms have been proposed based on the combination of the FBMV and DMAS beamforming algorithms. The numerical results showed the superior performance of the proposed method (DMAS_FBMV) where at the depth of 45 mm, the sidelobes were degraded about 12 dB compared to FBMV. In addition, at the depth of 25 mm, the SNR was improved about 5 dB by the DMAS_FBMV, and CR (at the depth of 15 mm) was enhanced about 7.2 dB, compared to FBMV. All the improvements were achieved at the expense of a higher computational complexity, but in the order of FBMV.

Nomenclature

β	isobaric volume expansion
$\Gamma(r)$	Gruneisen parameter
C_p	heat capacity

c	speed of sound
$A(r)$	spatial absorption
$I(t)$	temporal illumination functions
r_0	detector position
t	Time
$x_{id}(k)$	delayed detected signals
M	number of elements
L	subarray length
Δ	Δ
SNR	signal to noise
$FWHM$	full width half maximum
CR	contrast ratio

Subscript

d	Delay
-----	-------

References

- [1] M. Mehrmohammadi, S. Joon Yoon, D. Yeager, S. Y Emelianov, Photoacoustic imaging for cancer detection and staging, *Current molecular imaging*, 2(1) (2013) 89-105.
- [2] M. Nasiriavanaki, J. Xia, H. Wan, A.Q. Bauer, J.P. Culver, L.V. Wang, High-resolution photoacoustic tomography of resting-state functional connectivity in the mouse brain, *Proceedings of the National Academy of Sciences*, 111(1) (2014) 21-26.
- [3] R.O. Esenaliev, I.V. Larina, K.V. Larin, D.J. Deyo, M. Motamedi, D.S. Prough, Optoacoustic technique for noninvasive monitoring of blood oxygenation: a feasibility study, *Applied Optics*, 41(22) (2002) 4722-4731.
- [4] M. Heijblom, W. Steenbergen, S. Manohar, Clinical photoacoustic breast imaging: the twente experience, *IEEE pulse*, 6(3) (2015) 42-46.
- [5] N. Wu, S. Ye, Q. Ren, C. Li, High-resolution dual-modality photoacoustic ocular imaging, *Optics letters*, 39(8) (2014) 2451-2454.
- [6] M. Xu, L.V. Wang, Time-domain reconstruction for thermoacoustic tomography in a spherical geometry, *IEEE transactions on medical imaging*, 21(7) (2002) 814-822.
- [7] D. Feng, Y. Xu, G. Ku, L.V. Wang, Microwave-induced thermoacoustic tomography: Reconstruction by synthetic aperture, *Medical physics*, 28(12) (2001) 2427-2431.
- [8] M. Xu, L.V. Wang, Pulsed-microwave-induced thermoacoustic tomography: Filtered backprojection in a circular measurement configuration, *Medical physics*, 29(8) (2002) 1661-1669.
- [9] Y. Xu, D. Feng, L.V. Wang, Exact frequency-domain reconstruction for thermoacoustic tomography. I. Planar geometry, *IEEE transactions on medical imaging*, 21(7) (2002) 823-828.
- [10] M.A. Mastanduno, S.S. Gambhir, Quantitative photoacoustic image reconstruction improves accuracy in deep tissue structures, *Biomedical optics express*, 7(10) (2016) 3811-3825.
- [11] B.E. Treeby, T.K. Varslot, E.Z. Zhang, J.G. Laufer, P.C. Beard, Automatic sound speed selection in photoacoustic image reconstruction using an autofocus approach, *Journal of biomedical optics*, 16(9) (2011) 090501.
- [12] C. Huang, K. Wang, L. Nie, L.V. Wang, M.A. Anastasio, Full-wave iterative image reconstruction in photoacoustic tomography with acoustically inhomogeneous media, *IEEE transactions on medical imaging*, 32(6) (2013) 1097-1110.
- [13] C. Jia, W.C. Vogt, K.A. Wear, T.J. Pfefer, B.S. Garra, Two-layer heterogeneous breast phantom for photoacoustic imaging, *Journal of biomedical optics*, 22(10) (2017) 106011.
- [14] L. Li, L. Zhu, C. Ma, L. Lin, J. Yao, L. Wang, K. Maslov, R. Zhang, W. Chen, J. Shi, Single-impulse panoramic photoacoustic computed tomography of small-animal whole-body dynamics at high spatiotemporal resolution, *Nature biomedical engineering*, 1(5) (2017) 0071.
- [15] S. Schoeder, M. Kronbichler, W. Wall, Photoacoustic image reconstruction: material detection and acoustical heterogeneities, *Inverse Problems*, 33(5) (2017) 055010.
- [16] Y. Jiang, K. Pu, Advanced photoacoustic imaging applications of near-infrared absorbing organic nanoparticles, *Small*, 13(30) (2017) 1700710.
- [17] P.K. Upputuri, M. Pramanik, Fast photoacoustic imaging systems using pulsed laser diodes: a review, *Biomedical engineering letters*, 8(2) (2018) 167-181.
- [18] Y. Bai, B. Cong, X. Gong, L. Song, C. Liu, Compact and low-cost handheld quasibright-field linear-array probe design in photoacoustic computed tomography, *Journal of biomedical optics*, 23(12) (2018) 121606.
- [19] M. Mozaffarzadeh, A. Mahloojifar, V. Periyasamy, M. Pramanik, M. Orooji, Eigenspace-based minimum variance combined with delay multiply and sum beamformer: Application to linear-array photoacoustic imaging, *IEEE Journal of Selected Topics in Quantum Electronics*, 25(1) (2018) 1-8.
- [20] R. Paridar, M. Mozaffarzadeh, V. Periyasamy, M. Basij, M. Mehrmohammadi, M. Pramanik, M. Orooji, Validation of delay-multiply-and-standard-deviation weighting factor for improved photoacoustic imaging of sentinel lymph node, *Journal of biophotonics*, 12(6) (2019) e201800292.
- [21] M. Mozaffarzadeh, V. Periyasamy, M. Pramanik, B. Makkiabadi, Efficient nonlinear beamformer based on Pth root of detected signals for linear-array photoacoustic tomography: application to sentinel lymph node imaging, *Journal of biomedical optics*, 23(12) (2018) 121604.
- [22] K. Sivasubramanian, V. Periyasamy, M. Pramanik, Non-invasive sentinel lymph node mapping and needle guidance using clinical handheld photoacoustic imaging system in small animal, *Journal of biophotonics*, 11(1) (2018) e201700061.
- [23] M. Mozaffarzadeh, A. Mahloojifar, M. Orooji, S. Adabi, M. Nasiriavanaki, Double-stage delay multiply and sum beamforming algorithm: Application to linear-

- array photoacoustic imaging, *IEEE Transactions on Biomedical Engineering*, 65(1) (2018) 31-42.
- [24] M. Mozaffarzadeh, M.H.H. Varnosfaderani, A. Sharma, M. Pramanik, N. de Jong, M.D. Verweij, Enhanced Contrast Acoustic-Resolution Photoacoustic Microscopy using Double-Stage Delay-Multiply-and-Sum Beamformer for Vasculature Imaging, *Journal of biophotonics*, (2019).
- [25] M. Mozaffarzadeh, A. Hariri, C. Moore, J.V. Jokerst, The double-stage delay-multiply-and-sum image reconstruction method improves imaging quality in a led-based photoacoustic array scanner, *Photoacoustics*, 12 (2018) 22-29.
- [26] G. Matrone, A.S. Savoia, G. Caliano, G. Magenes, The delay multiply and sum beamforming algorithm in ultrasound B-mode medical imaging, *IEEE transactions on medical imaging*, 34(4) (2014) 940-949.
- [27] J.-F. Synnevag, A. Austeng, S. Holm, Benefits of minimum-variance beamforming in medical ultrasound imaging, *IEEE transactions on ultrasonics, ferroelectrics, and frequency control*, 56(9) (2009) 1868-1879.
- [28] S. Park, A.B. Karpouk, S.R. Aglyamov, S.Y. Emelianov, Adaptive beamforming for photoacoustic imaging, *Optics letters*, 33(12) (2008) 1291-1293.
- [29] M. Mozaffarzadeh, A. Mahloojifar, M. Orooji, K. Kratkiewicz, S. Adabi, M. Nasiriavanaki, Linear-array photoacoustic imaging using minimum variance-based delay multiply and sum adaptive beamforming algorithm, *Journal of biomedical optics*, 23(2) (2018) 026002.
- [30] B.M. Asl, A. Mahloojifar, Contrast enhancement and robustness improvement of adaptive ultrasound imaging using forward-backward minimum variance beamforming, *IEEE transactions on ultrasonics, ferroelectrics, and frequency control*, 58(4) (2011) 858-867.

Please cite this article using:

M. Mozaffarzadeh, S. A. O. Izadi Avajji, H. R. Jashnani, B-Mode Photoacoustic Imaging Using Linear Array: Numerical Study for Forward-Backward Minimum Variance Beamformer Combined with Delay-Multiply-and-Sum, *AUT J. Elec. Eng.*, 51(1) (2019) 21-28.
DOI: 10.22060/ej.2019.14025.5201



